 ©2021 Kvantovaya Elektronika and IOP Publishing Limited

LASER BIOPHOTONICS

https://doi.org/10.1070/QEL17503

Analytical model of fluorescence intensity for the estimation of fluorophore localisation in biotissue with dual-wavelength fluorescence imaging

A.V. Khilov, E.A. Sergeeva, D.A. Kurakina, I.V. Turchin, M.Yu. Kirillin

Abstract. **Analytical expression for the fluorescence response of a photosensitiser uniformly distributed in the superficial layer of biotissue is obtained in the diffusion approximation of radiative transfer theory, and the approach for estimating the fluorescent layer thickness based on dual-wavelength excitation of fluorescence is proposed. It is shown that the error in estimation of the fluorescent layer thickness employing the ratio of the fluorescence signals obtained at different excitation wavelengths does not exceed 30% for the thickness range of 0.1–2 mm in the case of 30%-variation of biotissue optical properties.**

Keywords: *radiative transfer theory, Monte Carlo simulations, fluorescence imaging, photodynamic therapy, chlorin-based photosensitisers.*

1. Introduction

Fluorescence imaging (FI) is one of the most actively developing trends in non-invasive diagnostics of biological tissues, which is currently being employed in various biomedical applications [1–3]. FI covers a wide range of instrumental imaging techniques and, in general, consists in the registration of spatial distribution of fluorescence intensity excited in biotissue by probing radiation. An important problem of quantitative FI consists in the estimation of localisation of fluorophores in biotissue. In particular, estimation of the thickness and the embedding depth of biotissue layers labelled with a fluorescence marker plays an important role in the detection of experimental tumours and metastases, sentinel lymph nodes [4], as well as in optimisation of photodynamic therapy (PDT) protocols [5]. A possible solution to this problem is provided by the diffusion fluorescence tomography (DFT) technique [6] applying iterative algorithms to reconstruct fluorophore concentration spatial distribution from the fluorescence images. The initial data for such algorithms is a set of fluorescence images obtained at different positions of the probing light source and the detector, the latter being typically a CCD matrix, or a photomultiplier, etc. [7–10]. Significant drawbacks of the DFT technique are (i) poor conditioning of the inverse problem [11, 12], especially in case when trans-illumination geometry measurements are unavailable; and (ii) complex technical implementation. These drawbacks significantly limit the employment of this technique in preclinical studies and especially in clinical practice. In this regard, currently DFT is primarily employed in experimental medicine where typical objects under study are small laboratory animals, while the range of clinical applications is significantly limited due to the complexity of trans-illumination geometry measurements. Thus, the problem of quantitative estimation of fluorophore localisation in biotissue remains important. FI techniques not requiring reconstruction which are widely employed in clinical practice offer a more simple and convenient solution. They are based on the registration of fluorescence intensity spatial distribution at biotissue surface employing CCD cameras upon broad-beam tissue illumination [4, 13]. However, this approach does not allow an explicit estimation of the fluorophore embedding depth.

For the estimation of the in-depth-fluorophore distribution within biotissues, a ratiometric approach can be employed, which implies registration of fluorescence signals corresponding to two or more different wavelengths of excitation or emission at which biotissue optical properties significantly differ. In papers [14–17] it was shown by Monte Carlo (MC) modelling and in model experiments with a fluorophore layer embedded in a biotissue phantom that the ratio of fluorescence signals corresponding to different emission wavelengths and same excitation wavelength can be employed to estimate the fluorophore embedding depth in biotissues. Theoretical description of dual-wavelength detection of fluorescence excited at the same wavelength is given in [18] using the diffusion approximation of the radiation transfer equation (RTE). Such an approach can be implemented by simultaneous registration of fluorescence responses at different wavelengths by a simple detector, e.g., a spectrometer. However, a large number of fluorophores are characterised by a small width of the emission spectral band, which leaves little possibility to resolve two or more detection lines (for example, the mKate protein fluorescence spectrum FWHM is 90 nm) and, therefore, limits the abilities of this approach.

Ratiometric approach in dual-wavelength FI can be realised with the use of fluorophores characterised by a broad absorption spectrum (or having several separated peaks in absorption spectrum) and by analysing fluorescence signals at different excitation wavelengths registered at the same emission wavelength. Examples of such fluorophores include chlorin-based photosensitisers (PS's) [19, 20] with two pronounced peaks in the absorption spectrum corresponding to wavelengths of 402 and 662 nm (Fig. 1), protoporphyrin IX (PPIX) [21, 22] characterised by a pronounced peak in the absorption spectrum at a wavelength of 405 nm and several less pronounced peaks at wavelengths in the range

A.V. Khilov, E.A. Sergeeva, D.A. Kurakina, I.V. Turchin, M.Yu. Kirillin Institute of Applied Physics, Russian Academy of Sciences, ul. Ul'yanova 46, 603950 Nizhny Novgorod, Russia; e-mail: alhil@inbox.ru

Received 7 December 2020
Kvantovaya Elektronika **51** (2) 95–103 (2021)
Translated by M.Yu. Kirillin

450–650 nm, and PEGylated chitosan nanoparticles with embedded bismuth sulfide BSA-Bi_2S_3-CG-PEG with a broad absorption spectrum [23]. Paper [24] presents the results of clinical studies of ratiometric endoscopic measurements of PPIX fluorescence in normal bladder tissue and in benign and malignant tumours of the same localisation. Difference in the values of fluorescence intensity ratio corresponding to excitation in the red and blue wavelength ranges was demonstrated for normal tissue, inflammation, dysplasia, non-invasive papillary carcinoma and carcinoma *in situ*. The results of fluorescence measurements were confirmed by the results of histological studies. The feasibility of the estimation of fluorophore embedding depth based on ratiometric fluorescence measurements with dual-wavelength excitation and dual-wavelength registration of fluorescence was shown in [25] for the fluorescein isothiocyanate based marker LS903. Note that the thickness of the fluorescent layer, along with its embedding depth in a biotissue, is also an important parameter which was not estimated in the above-mentioned works. The authors of the current study have previously demonstrated the possibility of estimating the chlorine-based PS localisation in a biotissue based on ratiometric imaging [26, 27] with dual-wavelength excitation and single-wavelength registration of fluorescence. FI of photosensitisers is essential for monitoring of their accumulation prior to a PDT procedure and their photobleaching in the course of irradiation [28–30].

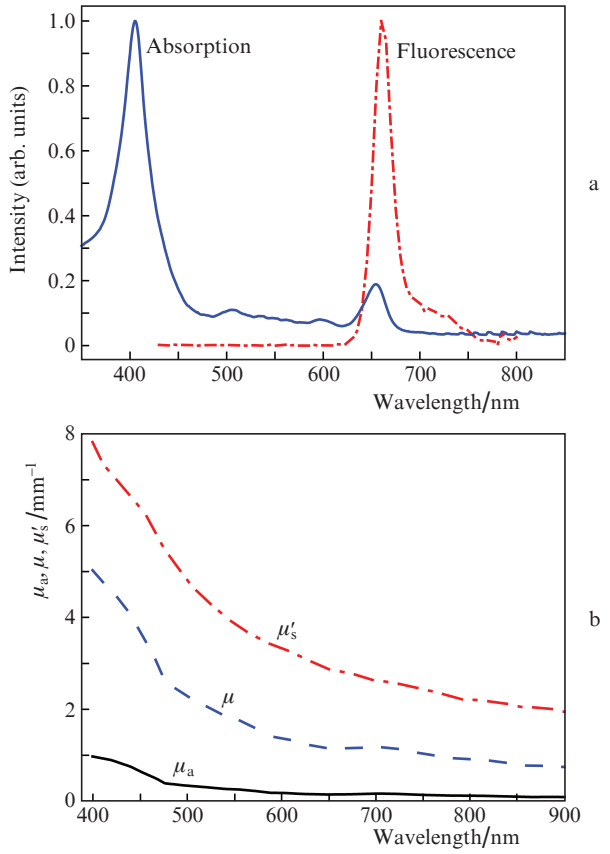

Figure 1. (a) Normalised absorption and emission spectra of chlorin-based PS's and (b) typical spectra of absorption coefficient μ_a, reduced scattering coefficient μ_s' and diffuse attenuation coefficient μ calculated by formula (5) for human dermis in the visible spectral range according to [31].

In this paper, a previously proposed approach to estimate the localisation of a chlorin-based PS in biotissues is further developed. It is based on dual-wavelength FI with the probing wavelengths corresponding to the peaks in the PS absorption spectrum located in different bands of the optical range in which light absorption by biotissues differs significantly. The method for estimating the thickness of the biotissue superficial fluorescent layer based on dual-wavelength FI is proposed. Estimation is based on the analytical model of fluorescence intensity distribution employing the diffusion approximation of RTE. Analytical results for dermis are confirmed by the results of MC modelling, which opens up the possibility of employing the developed model for estimation of the parameters of PS accumulation in biotissue superficial layer based on FI data in the course of a PDT procedure.

2. Materials and methods

2.1. Analytical model for fluorescence intensity detected from a fluorophore distributed in a superficial layer of biotissue

Calculation of fluorescence intensity from a fluorophore distributed in biotissue superficial layer is presented as the superposition of two problems, namely, the calculation of the spatial distribution of the excitation radiation intensity absorbed by the fluorophore, and subsequent calculation of the fluorescence intensity emitted by the fluorophore and registered at the biotissue surface. Biological tissue is considered as a semi-infinite two-layer medium containing a fluorophore with a fluorescence quantum yield η and a concentration C uniformly distributed in a thin superficial layer of thickness d. Illumination is performed with a wide excitation beam with a uniformly distributed intensity I_0 at the medium boundary $z = 0$ (Fig. 2). Biotissue is characterised by the absorption coefficient $\mu_{a\,tiss}(\lambda)$, scattering coefficient $\mu_s(\lambda)$, and anisotropy factor g. The absorption coefficient within the fluorescent layer is represented by a sum of the coefficients of intrinsic biotissue absorption and fluorophore absorption μ_{af} proportional to the concentration of the fluorophore: $\mu_a(\lambda) = \mu_{a\,tiss}(\lambda) + \mu_{af}(\lambda)$. For calculation of the radiation propagation it is assumed that additional absorption introduced by the fluorophore is small at both excitation wavelengths in comparison with the intrinsic absorption of biological tissue $\mu_{af}(\lambda) \ll \mu_{a\,tiss}(\lambda)$; fluorophore absorption at the emission

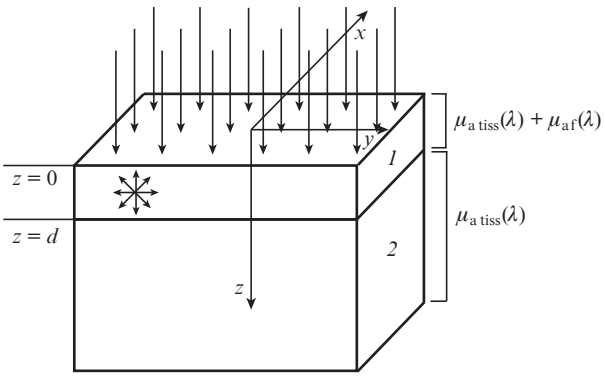

Figure 2. Medium geometry employed in analytical and numerical models [(*1*) biotissue layer containing a fluorophore, and (*2*) biotissue].

wavelength can be neglected compared to the biotissue absorption.

The intensity of the fluorescence emitted from the medium at the wavelength λ_{em} and registered at point $\boldsymbol{r}_0$ of the tissue surface (in the plane $z = 0$) upon irradiation of the superficial fluorescent layer is given in the form of integral over the superficial layer volume V:

$$I_{em}(\boldsymbol{r}_0,\lambda_{ex},\lambda_{em}) = \gamma \int_V \eta \Phi_{em}(\boldsymbol{r}_0,\boldsymbol{r},\lambda_{em})\, dP_{abs}(\boldsymbol{r},\lambda_{ex}), \quad (1)$$

where $dP_{abs}(\boldsymbol{r}, \lambda_{ex})$ is the excitation radiation power at a wavelength λ_{ex} absorbed by fluorophore in the elementary volume dV centred at point $\boldsymbol{r}$ of the tissue; γ is a factor associated with a refractive index mismatch at the tissue boundary; and $\Phi_{em}(\boldsymbol{r}_0, \boldsymbol{r}, \lambda_{ex})$ is the fluence rate generated at point $\boldsymbol{r}_0$ with a unit power source located at point $\boldsymbol{r}$. Elementary absorbed power $dP_{abs}(\boldsymbol{r}, \lambda_{ex})$ is expressed via local values of the fluence rate $\Phi_{ex}(\boldsymbol{r}, \lambda_{ex})$ in a medium and the absorption coefficient of the fluorophore in the form

$$dP_{abs}(\boldsymbol{r},\lambda_{ex}) = \mu_{af}(\boldsymbol{r},\lambda_{ex})\Phi_{ex}(\boldsymbol{r},\lambda_{ex})dV. \quad (2)$$

Distribution of excitation radiation absorbed by the fluorophore [the calculation of function $\Phi_{ex}(\boldsymbol{r}, \lambda_{ex})$] can be obtained using the analytical semi-empirical model presented in [32]. It is shown that for a semi-infinite layer of biotissue irradiated with a plane wave at a wavelength λ with intensity I_0, the fluence rate at depth z calculated by numerical MC simulations can be approximated by an exponential function for a wide range of tissue optical properties:

$$\Phi(z) = I_0 k \exp(-\mu z), \quad (3)$$

where k is the backscattering factor, and μ is the diffuse attenuation coefficient of the incident irradiation at a wavelength λ in the tissue. For these parameters the following empirical expressions are given which were obtained by fitting the results of MC simulation with the asymptotic solutions of the RTE:

$$k = 3 + 5.4R_d - 2\exp(-17R_d), \quad (4)$$

$$\mu = \tilde{\mu}\left[1 - \frac{\exp(-20R_d)}{\sqrt{3}}\right], \quad (5)$$

$$R_d \approx \exp\left(-8\frac{\mu_a}{\tilde{\mu}}\right), \quad (6)$$

where R_d is the total diffuse reflection parameter; $\tilde{\mu} = \sqrt{3\mu_a(\mu_a + \mu_s')}$ is the effective attenuation coefficient of diffuse light; and $\mu_s' = \mu_s(1 - g)$ is the reduced scattering coefficient in the tissue. The R_d and k values are calculated in [32] assuming that there is a refractive index mismatch $n = n_{medium}/n_{out} = 1.37$ at the biotissue surface (n_{medium} is biotissue refractive index and n_{out} is the surrounding medium refractive index). The typical spectrum of the attenuation coefficient μ for human dermis calculated by formula (5) using the absorption and scattering spectra from [31] is shown in Fig. 1b.

We introduce a broad-beam fluence rate Φ_{ex} in a tissue at a depth z described by formula (3):

$$\Phi_{ex}(z, \lambda_{ex}) = I_0 k_{ex} \exp(-\mu_{ex} z), \quad (7)$$

where $k_{ex} = k(\lambda_{ex})$, and $\mu_{ex} = \mu(\lambda_{ex})$.

Assuming that an elementary volume of a fluorophore located at point $\boldsymbol{r}(x, y, z)$ is an isotropic point source with power $\eta dP_{abs}(\boldsymbol{r}, \lambda_{ex})$, the intensity of its fluorescence registered at the outer boundary of the tissue at point $\boldsymbol{r}_0(x_0, y_0, 0)$ is presented in the form

$$dI_{em}(\lambda_{ex}, \lambda_{em}, \boldsymbol{r}, \boldsymbol{r}_0) = \gamma\eta dP_{abs}(\boldsymbol{r}, \lambda_{ex})\Phi_{em}(\boldsymbol{r}, \boldsymbol{r}_0, \lambda_{em}). \quad (8)$$

Here,

$$\Phi_{em}(\boldsymbol{r},\boldsymbol{r}_0,\lambda_{em}) = \frac{1}{4\pi D_{em}} \times\left\{\frac{\exp[-\tilde{\mu}_{em}\sqrt{(x-x_0)^2+(y-y_0)^2+z^2}]}{\sqrt{(x-x_0)^2+(y-y_0)^2+z^2}} - \frac{\exp[-\tilde{\mu}_{em}\sqrt{(x-x_0)^2+(y-y_0)^2+(z+2z_{em}^*)^2}]}{\sqrt{(x-x_0)^2+(y-y_0)^2+(z+2z_{em}^*)^2}}\right\} \quad (9)$$

is the fluence rate produced by an isotropic point source in a semi-infinite medium calculated in diffusion approximation of RTE [33];

$$D_{em} = \frac{1}{3[\mu_a(\lambda_{em}) + \mu_s'(\lambda_{em})]} = \frac{\mu_a(\lambda_{em})}{\tilde{\mu}_{em}^2}$$

is the diffusion coefficient at wavelength λ_{em}; $\tilde{\mu}_{em} = \tilde{\mu}(\lambda_{em})$; and $z_{em}^* = m\frac{2}{3}l_{tr}$ is the extrapolated length in the Milne problem ($\frac{2}{3}l_{tr} = 2D_{em}$) multiplied by factor m accounting for the refractive index mismatch n [33]. The multiplicative factor m is determined in accordance with formula (2.4.1) of paper [33] through integral transformations of the Fresnel energy reflection coefficient for a given relative refractive index n. Note that the factor γ from expressions (1), (8) and (9) is related to m as $\gamma = 1/(2m)$.

For uniform distribution of a fluorophore along transverse coordinates (x, y) and arbitrary in-depth (z axis) distribution assuming the excitation and fluorescence field perturbations introduced by the fluorophore are small, in accordance with the formulae (7)–(9), the fluorescence intensity registered at an arbitrary point of the tissue outer boundary after integration over transverse coordinates has the form of a one-dimensional integral:

$$I_{em}(\lambda_{ex},\lambda_{em}) = \gamma\frac{\eta I_0 k(\lambda_{ex})}{2\tilde{\mu}_{em}D_{em}}\int_{z=0}^{\infty}\mu_{af}(z,\lambda_{ex})\exp(-\mu_{ex}z) \times\{\exp(-\tilde{\mu}_{em}z) - \exp[-\tilde{\mu}_{em}(z+2z_{em}^*)]\}dz. \quad (10)$$

In the case of uniform fluorophore in-depth distribution within a layer of thickness d, the intensity of the registered fluorescence is expressed by the formula

$$I_{em}(\lambda_{ex},\lambda,d) = I_0\eta\mu_{af}(\lambda_{ex})K(\lambda_{ex},\lambda_{em}) \times\{1 - \exp[-(\mu_{ex} + \tilde{\mu}_{em})d]\}, \quad (11)$$

where

$$K(\lambda_{ex},\lambda_{em}) = \gamma \frac{k_{ex}(\lambda_{ex})\sinh(\tilde{\mu}_{em} z^*_{em})\exp(-\tilde{\mu}_{em} z^*_{em})}{\tilde{\mu}_{em} D_{em}(\mu_{ex}+\tilde{\mu}_{em})}.$$

From (11) it follows that the magnitude of the fluorescence signal increases monotonically with increasing fluorescent layer thickness and tends asymptotically to the constant $I^{(\infty)}_{em} = I_0 \eta \mu_{af}(\lambda_{ex}) K(\lambda_{ex},\lambda_{em})$. Such a dependence of the fluorescence signal is associated with a limited penetration depth of the excitation radiation in biotissue. For thin fluorescent layers which thickness satisfies the relation $(\mu_{ex}+\tilde{\mu}_{em})d \ll 1$, the registered fluorescence signal linearly depends on the layer thickness: $I_{em}(\lambda_{ex},\lambda_{em},d) \approx I_0 \eta \mu_{af} K(\lambda_{ex},\lambda_{em})(\mu_{ex}+\tilde{\mu}_{em})d$. The sensitivity range of the fluorescence signal to the presence of a fluorophore determined by the 95% level of a maximum value of $I^{(\infty)}_{em}$ is limited by the depth range $z \lesssim 3/(\mu_{ex}+\tilde{\mu}_{em})$, and the presence of a fluorophore outside these limits practically does not affect the change of the fluorescence signal. As follows from Fig. 1b, human dermis is characterised by higher values of the effective coefficient μ_{ex} in the range of the 'blue' chlorin-based PS absorption peak (λ_{ex1} is in the vicinity of 405 nm) as compared to the range of the 'red' peak (λ_{ex2} is in the vicinity of 660 nm): $\mu_{ex}(405)/\mu_{ex}(660) \approx 3.8$. Consequently, the saturation of the fluorescence signal excited in the blue range occurs at smaller depths, since the superficial region of strongly absorbing and scattering biotissue shields the penetration of probing radiation into deeper PS-containing layers.

2.2. Dual-wavelength fluorescence signals ratio and its relationship with the thickness of the PS-containing layer

For fluorophores with a broad absorption spectrum or with several peaks in the absorption spectrum, in particular, for a chlorin-based PS, the ratio of signals corresponding to two fluorescence excitation wavelengths normalised by the incident intensity can be introduced as:

$$R_\lambda = \frac{I_{em}(\lambda_{ex2},\lambda_{em},d)/I_0(\lambda_{ex2})}{I_{em}(\lambda_{ex1},\lambda_{em},d)/I_0(\lambda_{ex1})}. \quad (12)$$

Relation (12) is built in such a way that an increase in the layer thickness d corresponds to an increase in R_λ, while the denominator should contain the signal corresponding to larger attenuation coefficient values at the probing wavelength and, therefore, reaching saturation at lower d.

Taking into account relation (11), the expression for R_λ can be presented in the form:

$$R_\lambda = \frac{\eta_2 \mu_{af}(\lambda_{ex2}) k_{ex}(\lambda_{ex2})}{\eta_1 \mu_{af}(\lambda_{ex1}) k_{ex}(\lambda_{ex1})} \frac{\mu_{ex1}+\tilde{\mu}_{em}}{\mu_{ex2}+\tilde{\mu}_{em}} \times \frac{1-\exp[-(\mu_{ex2}+\tilde{\mu}_{em})d]}{1-\exp[-(\mu_{ex1}+\tilde{\mu}_{em})d]}, \quad (13)$$

where η_1 and η_2 are fluorescence quantum yields for excitation wavelengths λ_{ex1} and λ_{ex2}, respectively. The relation for R_λ depends only on tissue and fluorophore parameters and can be obtained from experimental measurements of fluorescence signals excited at two wavelengths, provided that the characteristics of the registering equipment at these wavelengths do not differ, or after normalisation for the corresponding detection parameters.

Using formula (13) one can analyse the asymptotic behaviour of R_λ at small and large fluorescent layer thicknesses d. For $d \to 0$, the fluorescence signals excited at both wavelengths linearly depend on the thickness and, as a result, R_λ tends to a constant value

$$R_\lambda(d \to 0) \approx R^{(0)}_\lambda = \frac{\eta_2 \mu_{af}(\lambda_{ex2}) k_{ex}(\lambda_{ex2})}{\eta_1 \mu_{af}(\lambda_{ex1}) k_{ex}(\lambda_{ex1})}. \quad (14)$$

Note that $R^{(0)}_\lambda$ is expressed via the product of two values: the ratio of the reduced PS absorption coefficients $\eta\mu_a$ at two excitation wavelengths and the ratio of the normalised intensities of probing radiation at the medium surface $k_{ex}(\lambda_{ex2})/k_{ex}(\lambda_{ex1})$ which can be directly measured as back-reflectance intensities. For small values of d, the dependence $R_\lambda(d)$ is close to a linear one which slope is determined by the difference in the attenuation coefficients of the excitation radiation at two wavelengths:

$$R_\lambda(d) \approx R^{(lin)}_\lambda(d) = R^{(0)}_\lambda[1 + d(\mu_{ex1}-\mu_{ex2})/2]. \quad (15)$$

This asymptotic describes well the behaviour of $R_\lambda(d)$ in the range of values $0 < d < 2/(\mu_{ex1}-\mu_{ex2})$; when the thickness of a PS-containing layer goes beyond this interval, the growth of $R_\lambda(d)$ slows down, and for large thicknesses the ratio tends to a constant value

$$R_\lambda(d \gg 2/(\mu_{ex1}-\mu_{ex2})) \approx R^{(\infty)}_\lambda = R^{(0)}_\lambda \frac{\mu_{ex1}+\tilde{\mu}_{em}}{\mu_{ex2}+\tilde{\mu}_{em}}. \quad (16)$$

This limit value depends on the attenuation coefficient at the emission wavelength, in contrast to characteristics (14), (15) for small d determined by the attenuation parameters of probing radiation only and the reduced PS absorption coefficients. Based on the condition $R_\lambda \lesssim 0.95 R^{(\infty)}_\lambda$, the ratio R_λ is sensitive to the thickness of the PS-containing layer in the range of values $0 < d < 3/(\mu_{ex2}+\tilde{\mu}_{em})$ and can be employed for the estimation of the fluorescent layer thickness if the spectra of the PS reduced absorption coefficient $\eta\mu_{af}$ and attenuation coefficient μ (as a general case of $\tilde{\mu}$) are known.

3. Monte Carlo simulations

For numerical confirmation of the developed theoretical model and, in particular, the dependence $R_\lambda(d)$, we performed MC simulations of the fluorescence intensity from the fluorophore distributed in the biotissue superficial layer tissue. The simulation algorithm has been adapted for the MATLAB environment. Since the MATLAB environment is optimised for large arrays, simultaneous operations with the arrays of photon parameters are time-saving compared to traditional sequential calculation of random trajectories [26, 34]. In accordance with the scheme in Fig. 2, the biological tissue was defined as a two-layered medium with an upper layer containing a uniformly distributed chlorin-based PS with a volume concentration of $C = 0.5\%$. The selected value of the fluorophore concentration corresponds to the typical values of PS accumulation after topical administration prior to a PDT procedure [35]. The thickness of the fluorescent layer varied from 0.01 to 3 mm, while the total thickness of the biotissue sample was 6 mm. The transverse dimensions of the sample were 20 × 20 mm. Fluorescence was excited by a wide and spatially uniform collimated beam at a wavelength of 405 or 660 nm, corresponding to absorption peaks of a chlorin-based PS. Basic optical parameters of biological tissue for MC simulations corresponded to the parameters of human

Table 1. Basic dermis optical properties employed for MC simulations and analytical studies adopted from paper [31].

Wavelength	μ_a/mm^{-1}		μ_s/mm^{-1}	g	μ/mm^{-1}	
	Biotissue	Layer with a PS			Biotissue	Layer with a PS
λ_{ex1} = 405 nm	0.89	1.01	37	0.80	4.67	4.99
λ_{ex2} = 660 nm	0.15	0.19	14	0.80	1.15	1.31
λ_{em} = 760 nm	0.13	0.13	12	0.80	0.96	0.96

dermis [31] (Table 1). The refractive index of biotissue was equal to 1.37. To demonstrate the sensitivity of the fluorescence signal characteristics to biotissue optical properties we additionally performed modelling with the variations of absorption and scattering coefficients by 30% relative to the base values, both upward and downward.

The modelling of the fluorescence response from the PS-containing layer was implemented in two stages, similar to the construction of the analytical model (AM). At the first stage, three-dimensional light dose absorption maps $P_{abs}(\lambda_{ex}, x_i, y_i, z_i)$ were calculated for both values of excitation wavelength λ_{ex} for the given tissue geometry, spatial fluorophore distribution, and optical properties of the tissue and fluorophore. Additional absorption in the PS-containing layer was taken into account in the simulations. At the second stage, the calculated map of the absorbed light dose was treated as a distribution of fluorescence sources. Total weight of fluorescence photons emitted from the centre of each voxel of the map was equal to $\eta P_{abs}(\lambda_{ex}, x_i, y_i, z_i) \times \Delta x \Delta y \Delta z$, where Δx, Δy, and Δz are voxel sizes over three coordinates. The voxel sizes Δx, Δy, and Δz were equal to 0.25, 0.25, and 0.01 mm, respectively. Larger discretisation over z axis is due to the fact that fluorescence photons are emitted from the centre of the voxel, which requires determination of the elementary source depth with higher accuracy, while for the transversely uniform problem the accuracy in the (x, y) position of the source is not that critical. Emission of fluorescence photons was assumed isotropic in direction, and the dependence of the fluorescence quantum yield on the excitation wavelength was not taken into account, and we additionally assumed $\eta_1 = \eta_2 = 1$.

Simulation of fluorescence photon propagation at the second stage was performed for a medium with optical properties corresponding to the emission wavelength λ_{em}, and surface distribution of the weight of photons emitted from biotissue in accordance with the refraction law was calculated on the outer side of the biotisuue interface with $z = 0$. Fluorescence photons with the total weight $P_{abs}(\lambda_{ex}, x_i, y_i, z_i)\Delta x \Delta y \Delta z$ were emitted from each point corresponding to the absorption map voxel centre.

The resulting fluorescence intensity was calculated by averaging the total weight of photons leaving the tissue over an area of 5×5 mm, similar to signal processing in the experiment described in [36]. The ratio of fluorescence signals $R_\lambda(d)$ excited at two wavelengths was calculated from the modelling results in accordance with expression (12).

4. Results and discussion

Results of analytical calculation of dual-wavelength fluorescence characteristics of a PS-containing layer of thickness d embedded in biological tissue together with the results of MC simulations are presented in Fig. 3 for basic optical parameters of biological tissue [31] given in Table 1. Fluorescence signals at a wavelength of 760 nm corresponding to the excitation wavelengths of 405 and 660 nm are shown in Figs 3a and 3b, respectively. For analytical calculations, similar to MC simulations, it was assumed that the fluorescence quantum yield does not depend on the wavelength and is equal to unity. Since the problem considers a two-layer medium with a PS-containing upper layer, while analytical solutions were obtained within the framework of radiation propagation in a homogeneous medium, analytical curves are given for two cases: (i) total absorption coefficient of the sample at the excitation wavelength is equal to that of pure biotissue $[\mu_{a\,tiss}(\lambda)]$ or (ii) total absorption coefficient of the sample is the sum of biotissue and PS absorption coefficient $[\mu_{a\,tiss}(\lambda) + \mu_{af}(\lambda)]$.

As it can be seen from Figs 3a and 3b, the fluorescence intensity reaches the limit value $I_{em}^{(\infty)}$ faster for the excitation wavelength of 405 nm, which is associated with stronger attenuation of the probing radiation at this wavelength compared to the wavelength of 660 nm. At the same time, the asymptotic level of fluorescence intensity calculated by MC simulations is lower. This discrepancy is presumably due to a

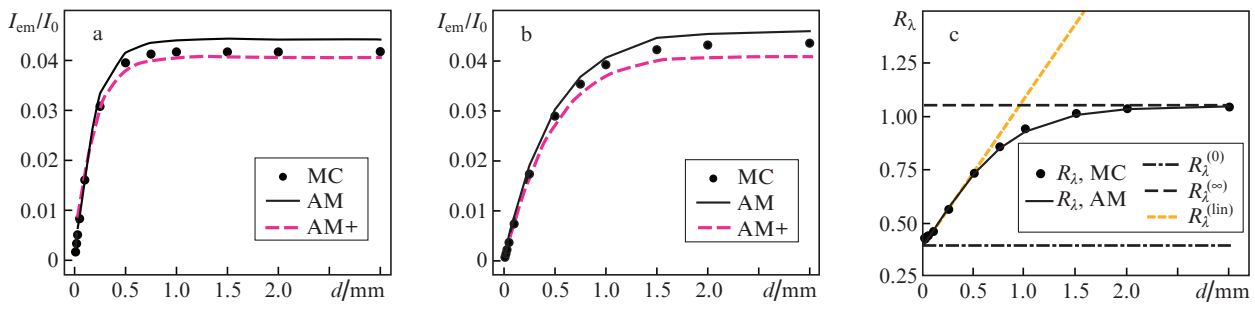

Figure 3. Fluorescence intensities I_{em}/I_0 normalised by the intensity of incident radiation as functions of the PS-containing surface layer thickness d upon excitation at wavelengths of (a) 405 and (b) 660 nm, and (c) ratios R_λ for the entire considered range of d, calculated by MC simulations (MC) and analytical model for basic dermis optical properties (AM) and for account of the PS contribution to the absorption coefficient $\mu_a(\lambda) = \mu_{a\,tiss}(\lambda) + \mu_{af}(\lambda)$ (AM+). Figure (c) also shows asymptotes of the dependence $R_\lambda(d)$.

simplification made in the analytical model (AM) when additional absorption in the PS-containing layer is neglected for both excitation and fluorescence wavelengths, and the tissue is considered to be homogeneous. To confirm this assumption, Fig. 3 and the following figures (see below) show additional analytical curves calculated by formula (11) for a homogeneous tissue with a uniformly distributed PS with a given concentration in the entire volume with the absorption coefficient $\mu_a(\lambda) = \mu_{a\,tiss}(\lambda) + \mu_{a\,f}(\lambda)$. Figure 3a and 3b demonstrate that the asymptotics of the fluorescence signal dependence on d calculated by MC simulation is located between the asymptotes calculated using AM for tissues with basic absorption and with account for additional PS contribution. The ratio $R_\lambda(d)$ calculated using relation (12) from the results of AM and MC modelling are shown in Fig. 3c along with asymptotes (14)–(16). The analytical model is in good agreement with the results of numerical simulations. However, it is necessary to note that for small d ($d < 0.1$ mm), the results of MC modelling differ from the linear asymptotic provided by AM, since for small values of d the applicability conditions of the diffusion approximation employed in AM are not satisfied. The demonstrated dependence indicates the presence of a linear section in the interval $d = 0.1–0.5$ mm, followed by transition to a constant asymptote. The $R_\lambda(d)$ value is less sensitive to a nonuniform absorption distribution (as to a higher-order effect).

The ratiometric parameter R_λ calculated by (12) allows adequate estimation of the thickness d of a chlorin-based PS-containing layer even with the described simplifications of the fluorescence signal model. Analytical calculation of R_λ with account for additional PS absorption in the whole biotissue volume does not seem appropriate, since owing to significant backscattering of 660-nm excitation light from the tissue volume below the PS layer, this approach would introduce a systematic error.

To estimate the sensitivity of the developed AM to the variations of biotissue optical properties, the comparison of the results of MC simulation and analytical study was performed for media with ±30% variations with respect to basic dermis optical properties. The results for the medium with the absorption coefficient variations within ±30% range are shown in Fig. 4.

Note that fluorescence signal from the tissue is formed not only by photons emitted from the upper PS-containing of layer of the tissue, but also by photons diffusely backscattered by the lower layer containing no PS. From the results presented in Figs 3 and 4, one can see that for $\lambda_{ex} = 405$ nm the dependence of the fluorescence signal on d calculated by MC simulations is closer to the analytical curve for tissue with increased absorption ($\mu_a = \mu_{a\,tiss} + \mu_{a\,f}$). It is due to the fact that blue-light excited fluorescence is formed primarily by superficial tissue layers and for large thicknesses of the PS-containing layer it is weakly sensitive to the parameters of the lower layer containing no PS. Upon red-light excitation ($\lambda_{ex} = 660$ nm), photons backscattered from the underlying tissue volume without a PS significantly contribute to the light dose absorbed by fluorophore; therefore, the fluorescence intensity curve calculated by Monte Carlo simulations is located between two analytical curves calculated for tissues with basic absorption and with additional PS absorption. This conclusion is confirmed by the results of calculations for the variations of scattering coefficient within ±30% range (results not shown due their similarity to the results for absorption coefficient variations). In case of simultaneous variations of absorption and scattering coefficients within ±30% range, the diffuse attenuation coefficient μ changes in the same range. Such a change in μ is more pronounced compared to the variations of scattering or absorption coefficients only, which leads to more significant changes in the behaviour of the $R_\lambda(d)$ dependence. The corresponding dependen-

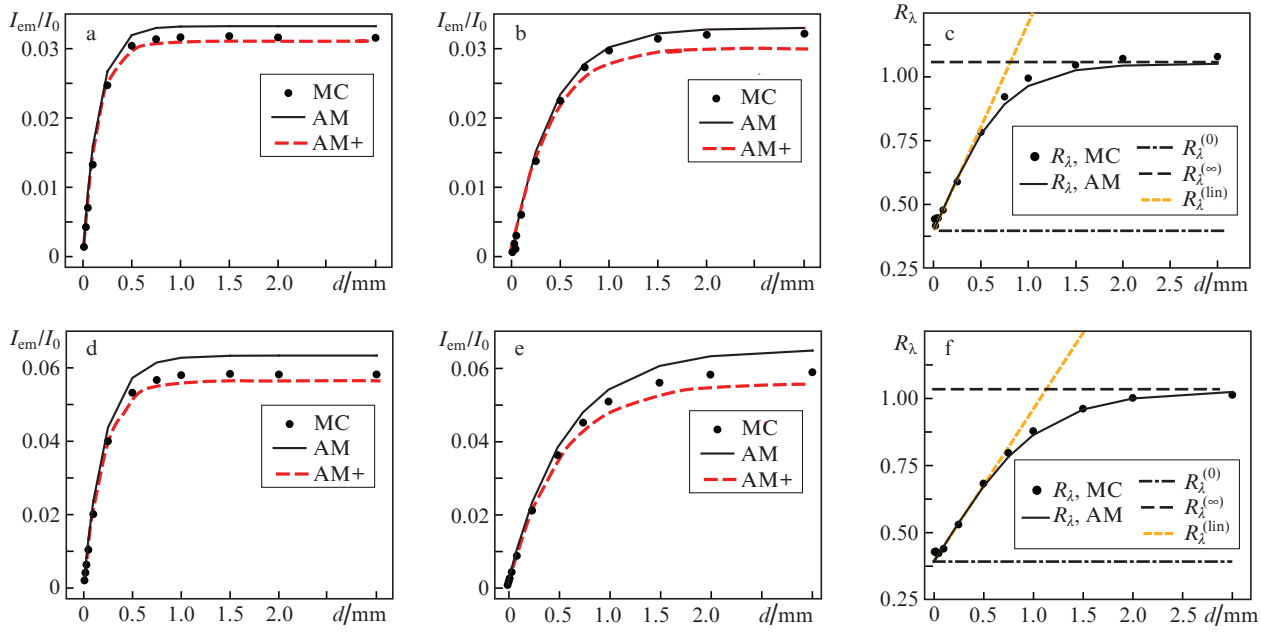

Figure 4. Fluorescence intensities I_{em}/I_0 normalised by the intensity of incident radiation as functions of the PS-containing superficial layer thickness d upon excitation at wavelengths of (a, d) 405 and (b, e) 660 nm, and (c, f) ratios R_λ calculated by MC simulations (MC) and analytical model without (AM) and with (AM+) account of the PS contribution of to biotissue absorption coefficient for relative variations in tissue absorption coefficients of (a–c) +30% and (d–f) –30% (Table 1).

cies are shown in Fig. 5. Since the slope of the $R_\lambda(d)$ dependence in the linear section is proportional to the difference $\mu_{ex1} - \mu_{ex2}$ (15); corresponding deviations of the dependences from the case of basic parameters are observed. It should be noted that the results of AM and MC simulations are in good agreement for all the cases considered.

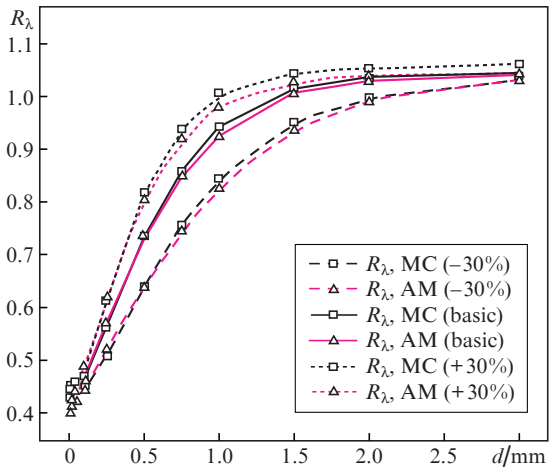

Figure 5. Ratios R_λ of fluorescence intensities at wavelengths of 660 and 405 nm, calculated by MC simulation and by AM for basic tissue parameters and for the cases of simultaneous variations of tissue absorption and scattering coefficients by ±30% relative to the baseline.

Analysis of the $R_\lambda(d)$ dependences in Figs 3–5 shows that a proportional variation of the basic tissue optical properties at both excitation wavelengths while keeping the shape of the PS absorption spectrum practically does not affect the range of $R_\lambda[R_\lambda^{(0)}, R_\lambda^{(\infty)}]$ values, since the latter is determined by the ratio of tissue properties at wavelengths λ_{ex1}, λ_{ex2}, and λ_{em} (13). The slope $R_\lambda(d)$ of the linear section, on the contrary, is sensitive to changes in the absolute values of the attenuation coefficients μ, since it is proportional to the difference $\mu_{ex1} - \mu_{ex2}$ (15); however, relative changes of the same magnitude and sign in either absorption or scattering coefficients lead to practically the same rate of change in $R_\lambda(d)$.

Obviously, for the estimation of the fluorescent layer thickness d from dual-wavelength FI measurements, it is necessary to employ the function $d(R_\lambda)$, which is the inverse of the above-mentioned dependence $R_\lambda(d)$; however, since the value of R_λ depends on tissue optical properties, the *a priori* unknown tissue optical properties can act as a source of error in estimation of d. For the estimation of this error, the $d(R_\lambda)$ dependences were plotted for basic optical properties and for the case of their variations within ±30% range. The estimation of the value range width (highlighted in Fig. 6 in gray) for fixed values of R_λ allows predicting the error in the estimation of the fluorescent layer thickness below 25%–30% with an uncertainty in determination of biotissue optical properties in 30% in the range of $R_\lambda = [0.4, 1]$ which corresponds to the range of fluorescent layer thicknesses $d \approx 0.1-2$ mm. For small values of d ($d \ll l_{tr} = 3D$), the described AM cannot be employed, since the applicability conditions for the diffusion approximation are violated.

The applicability of the proposed method for the estimation of fluorophore localisation is also limited by the condition $\mu_a \ll \mu_s'$ for the absorption coefficient and reduced scattering coefficient in biotissue (applicability condition for the diffusion approximation). If this condition is violated, formula (12) is not valid, and employment of MC simulations is reasonable for the estimation of fluorophore localisation. As we previously demonstrated [26, 27], the R_λ value can be employed for the estimation of the localisation of chlorin-based PS in biotissue if the values of μ_{ex1} and μ_{ex2} are significantly different.

It should be noted that the proposed model for the estimation of the PS-containing layer thickness is based on a simplifying assumption regarding the uniformity of the PS in-depth distribution. In practice, the concentration of the substance administered on the biotissue surface decreases with depth; moreover, typical PS penetration depth depends both on the matter diffusion characteristics and on the penetration time. The problem of determination of the PS spatiotemporal distribution in biotissue as a result of its diffusion was solved, for example, in paper [37]. To extend the developed here simplified principle of PS thickness layer evaluation onto a real situation of a nonuniform PS distribution, one can approximate a complex depth-dependence of PS concentration at each

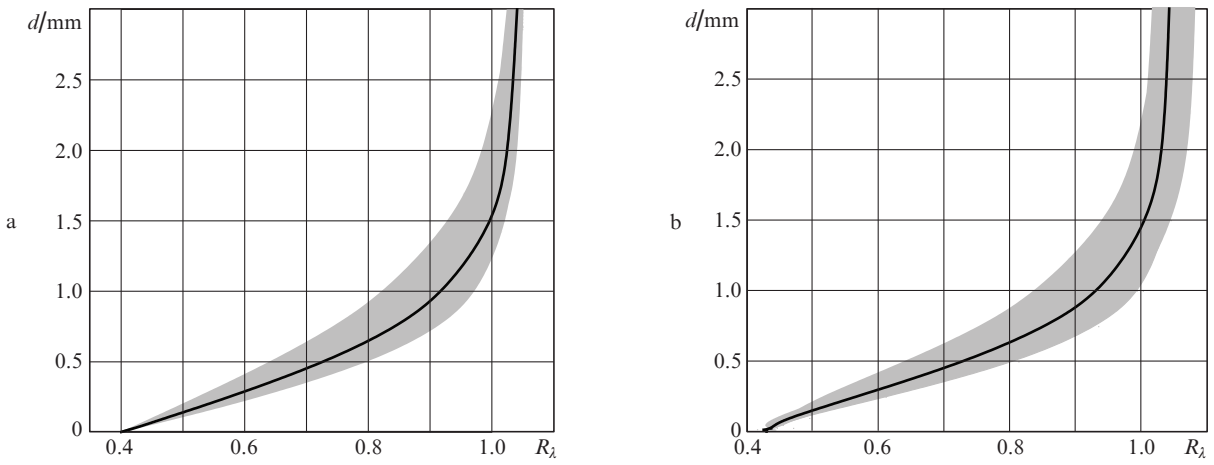

Figure 6. Estimations of the fluorescent layer thickness d based on the fluorescence signals ratio R_λ, obtained by (a) applying AM and (b) MC simulations for basic values of optical properties of dermis (solid curve) and for the cases of their variations (including simultaneous ones) within ±30% range (the interval is indicated in gray).

time moment by a step function with parameters (the thickness of the PS-containing layer and the absorption level of a PS) expressed through the characteristic in-depth decay scale of PS concentration and the value of PS concentration at the surface. In this situation the estimation of the PS-containing layer thickness by fluorescence ratiometric measurements will allow tracking the dynamics of PS penetration into biotissue and determining its characteristic temporal parameters, which is of practical value in monitoring of PS accumulation in various biotissues.

Traditionally, the studies of the fluorophore penetration into biotissues are mainly associated with the estimation of the average concentration, not with the measurements of their in-depth distribution. Non-invasive *in vivo* techniques for studying the fluorophores accumulation after topical administration can be differentiated into the methods of direct and indirect imaging. The first group includes confocal and multiphoton fluorescence microscopy [38, 39] characterised by cellular-resolution level and significantly limited imaging depth below 500 μm due to scattering in biotissue. The second group includes spectroscopic techniques [40] and DFT [6–11, 41], which have the imaging depth of up to tens of millimetres. The existing spectroscopic techniques do not imply estimation of the dye layer embedding depth, while the accuracy in estimation of the dye concentration is determined by the accuracy of the analytical model employed in the reconstruction algorithm. The DFT technique, which has been successfully implemented in recent years using hyperspectral technologies [41], has a submillimetre spatial resolution and allows reconstructing the fluorophore three-dimensional spatial distribution at depths of up to tens of millimetres. However, this is an extremely expensive [41] and time-consuming [10, 11] technique with significantly limited abilities for application in clinical practice. The technique proposed in our study for the estimation of the fluorescent layer thickness has such advantages as simplicity of technical implementation, economic efficiency and high potential for applications in biomedical research and clinical practice.

5. Conclusions

Within the frames of a semi-empirical model employing the diffusion approximation of radiative transfer theory, an analytical expression for fluorescence intensity detected from a fluorophore distributed in a biotissue superficial layer is obtained. On the basis of the proposed model, a method for the estimation of the fluorescent layer thickness was developed based on dual-wavelength ratiometric FI. It is shown that the results of analytical calculations of the detected fluorescence intensity are in good agreement with the results of MC simulations for the parameters corresponding to topical administration of PS's in a therapeutic concentration on human skin. It is shown that the ratio of the fluorescence signals obtained upon the excitation at two wavelengths allows estimating the thickness of the superficial skin layer containing uniformly distributed PS's in the range of 0.1–2 mm with accuracy no worse than 30% given a 30% variation in the determination of optical properties of biological tissue.

Quantitative estimation of the PS penetration depth based on the described model requires information about biotissue optical properties at all operating wavelengths. Simultaneous back-reflectance measurements and dual-wavelength FI with the evaluation of biotissue optical properties is a promising combination for the enhancement of the diagnostic value of the proposed technique preceding a PDT procedure.

Acknowledgements. This work was supported by the Russian Science Foundation (Project No. 17-15-01264).

References

1. Frangioni J.V. *Curr. Opin. Chem. Biol.*, **7** (5), 626 (2003).
2. Rao J., Dragulescu-Andrasi A., Yao H. *Curr. Opin. Biotechnol.*, **18** (1), 17 (2007).
3. Leblond F., Davis S.C., Valdés P.A., Pogue B.W. *J. Photochem. Photobiol. B*, **98** (1), 77 (2010).
4. Troyan S.L., Kianzad V., Gibbs-Strauss S.L., Gioux S., Matsui A., Oketokoun R., Ngo L., Khamene A., Azar F., Frangioni J.V. *Ann. Surg. Oncol.*, **16** (10), 2943 (2009).
5. Johansson T., Thompson M.S., Stenberg M., af Klinteberg C., Andersson-Engels S., Svanberg S., Svanberg K. *Appl. Opt.*, **41** (7), 1462 (2002).
6. Yang X., Gong H., Quan G., Deng Y., Luo Q. *Rev. Sci. Instrum.*, **81** (5), 054304 (2010).
7. Eppstein M.J., Hawrysz D.J., Godavarty A., Sevick-Muraca E.M. *Proc. Natl. Acad. Sci. USA*, **99** (15), 9619 (2002).
8. Milstein A.B., Oh S., Webb K.J., Bouman C.A., Zhang Q., Boas D.A., Millane R. *Appl. Opt.*, **42** (16), 3081 (2003).
9. Klose A.D., Hielscher A.H. *Opt. Lett.*, **28** (12), 1019 (2003).
10. Kleshnin M., Turchin I. *Laser Phys. Lett.*, **10** (7), 075601 (2013).
11. Fiks I., Kirillin M., Sergeeva E., Turchin I. *Radiophys. Quantum Electron.*, **54** (3), 197 (2011).
12. Shcherbo D., Merzlyak E.M., Chepurnykh T.V., Fradkov A.F., Ermakova G.V., Solovieva E.A., Lukyanov K.A., Bogdanova E.A., Zaraisky A.G., Lukyanov S. *Nat. Methods*, **4** (9), 741 (2007).
13. Vahrmeijer A.L., Hutteman M., Van Der Vorst J.R., van De Velde C.J., Frangioni J.V. *Nat. Rev. Clin. Oncol.*, **10** (9), 507 (2013).
14. Svensson J., Andersson-Engels S. *Opt. Express*, **13** (11), 4263 (2005).
15. Swartling J., Svensson J., Bengtsson D., Terike K., Andersson-Engels S. *Appl. Opt.*, **44** (10), 1934 (2005).
16. Jermyn M., Kolste K.K., Pichette J., Sheehy G., Angulo-Rodríguez L.M., Paulsen K.D., Roberts D.W., Wilson B.C., Petrecca K., Leblond F. *J. Biomed. Opt.*, **20** (3), 036014 (2015).
17. Wirth D., Kolste K., Kanick S., Roberts D.W., Leblond F., Paulsen K.D. *Biomed. Opt. Express*, **8** (8), 3656 (2017).
18. Leblond F., Ovanesyan Z., Davis S., Valdés P., Kim A., Hartov A., Wilson B., Pogue B., Paulsen K., Roberts D. *Phys. Med. Biol.*, **56** (21), 6823 (2011).
19. Spikes J.D. *J. Photochem. Photobiol. B*, **6** (3), 259 (1990).
20. Ol'shevskaya V.A., Nikitina R.G., Savchenko A.N., Malshakova M.V., Vinogradov A.M., Golovina G.V., Belykh D.V., Kutchin A.V., Kaplan M.A., Kalinin V.N. *Bioorg. Med. Chem.*, **17** (3), 1297 (2009).
21. Sternberg E.D., Dolphin D., Brückner C. *Tetrahedron*, **54** (17), 4151 (1998).
22. Kelty C.J., Brown N.J., Reed M.W., Ackroyd R. *Photochem. Photobiol. Sci.*, **1** (3), 158 (2002).
23. Wang K., Zhuang J., Liu Y., Xu M., Zhuang J., Chen Z., Wei Y., Zhang Y. *Carbohydr. Polym.*, **184**, 445 (2018).
24. Zaak D., Frimberger D., Stepp H., Wagner S., Baumgartner R., Schneede P., Siebels M., Knüchel R., Kriegmair M., Hofstetter A. *J. Urol.*, **166** (5), 1665 (2001).
25. Miller J.P., Maji D., Lam J., Tromberg B.J., Achilefu S. *Biomed. Opt. Express*, **8** (6), 3095 (2017).
26. Khilov A., Kirillin M., Loginova D., Turchin I. *Laser Phys. Lett.*, **15** (12), 126202 (2018).
27. Khilov A.V., Kurakina D.A., Turchin I.V., Kirillin M.Yu. *Quantum Electron.*, **49** (1), 63 (2019) [*Kvantovaya Electron.*, **49** (1), 63 (2019)].
28. Gamayunov S., Turchin I., Fiks I., Korchagina K., Kleshnin M., Shakhova N. *Photon. Laser Med.*, **5** (2), 101 (2016).

29. Kurakina D., Khilov A., Shakhova M., Orlinskaya N., Sergeeva E., Meller A., Turchin I., Kirillin M. *J. Biomed. Opt*., **25** (6), 063804 (2019).
30. Shakhova M., Loginova D., Meller A., Sapunov D., Orlinskaya N., Shakhov A., Khilov A., Kirillin M. *J. Biomed. Opt*., **23** (9), 091412 (2018).
31. Salomatina E.V., Jiang B., Novak J., Yaroslavsky A.N. *J. Biomed. Opt*., **11** (6), 064026 (2006).
32. Jacques S.L. *J. Biomed. Opt*., **15** (5), 051608 (2010).
33. Haskell R.C., Svaasand L.O., Tsay T.-T., Feng T.-C., McAdams M.S., Tromberg B.J. *J. Opt. Soc. Am*., **11** (10), 2727 (1994).
34. Kirillin M.Yu., Kurakina D.A., Perekatova V.V., Orlova A.G., Sergeeva E.A., Khilov A.V., Subochev P.V., Turchin I.V., Mallidi S., Hasan T. *Quantum Electron*., **49** (1), 43 (2019) [*Kvantovaya Electron*., **49** (1), 43 (2019)].
35. Khilov A.V., Loginova D.A., Sergeeva E.A., Shakhova M.A., Meller A.E., Turchin I.V., Kirillin M.Yu. *Sovr. Tekh. Med*., **9** (4), 96 (2017).
36. Kleshnin M., Fiks I., Plekhanov V., Gamayunov S., Turchin I. *Laser Phys. Lett*., **12** (11), 115602 (2015).
37. Svaasand L.O., Wyss P., Wyss M.-T., Tadir Y., Tromberg B.J., Berns M.W. *Lasers Surg. Med*., **18**, 139 (1996).
38. Huang A.Y., Myers J.T., Barkauskas D., Howell S.J., Oleinick N.L., McCormick T.S., Cooper K.D., Baron E.D., Lam M. *Photodiagn. Photodyn. Ther*., **9** (3), 225 (2012).
39. Lademann J., Meinke M., Schanzer S., Richter H., Darvin M., Haag S.F., Fluhr J., Weigmann H.-J., Sterry W., Patzelt A. *Int. J. Cosmet. Sci*., **34** (6), 551 (2012).
40. Genina E.A., Bashkatov A.N., Tuchin V.V. *Quantum Electron*., **44** (7), 689 (2014) [*Kvantovaya Electron*., **44** (7), 689 (2014)].
41. Dang X., Bardhan N.M., Qi J., Gu L., Eze N.A., Lin C.-W., Kataria S., Hammond P.T., Belcher A.M. *Sci. Rep*., **9**, 3873 (2019).